Fracture surface statistics of filled elastomers

Thomas Horst,[1,*] Katrin Reincke,[2] Sybill Ilisch,[2] Gert Heinrich,[1] and Wolfgang Grellmann[2]

[1]*Leibniz Institute of Polymer Research Dresden, Hohe Str. 6, D-01069 Dresden, Germany*
[2]*Martin Luther University Halle-Wittenberg, Center of Engineering Sciences, D-06099 Halle (Saale), Germany*

Roughness profiles of fracture surfaces formed as a result of the fast crack propagation through a filled rubber were analyzed by means of the height-height correlation functions. The fracture surface was found to be anisotropic in a certain domain of values of length scales; i.e., different values of roughness exponents are observed across and along the crack propagation direction. A two-dimensional analysis reveals a Family-Vicsek scaling in this domain characterized as well by two exponents. These characteristic values of the roughness exponents are found to be close to those observed for fracture surfaces of certain nonrubber materials at length scales smaller than the size of the fracture process zone. Hence, a ductile fracture process can be surmised to occur within the domain of the corresponding length scales.

I. INTRODUCTION

The fracture of a material involves a number of complex processes on multiple length scales. In materials science, increased fracture toughness can be achieved by modifying the structure of the material by way of inducing dissipative processes on various length scales, which result in increasing the energy adsorption accompanying the process of crack propagation through this material.

Elastomeric materials are weakly cross-linked polymers. Above the glass transition temperature, even weak external forces can cause large deformations of these materials owing to the high internal flexibility of network chains. These materials are typically blended with fillers in order to enhance their mechanical properties such as hardness, stiffness, or abrasion resistance.

Due to the large deformations, the deformed volume is about the magnitude of the specimen. Moreover, an elastic crack blunting can be observed; i.e., the crack opens up when the specimen is loaded. However, crack tip blunting is reversible in contrast to the plastic crack blunting in metallic materials. As a consequence, the stress and strain fields in the vicinity of the crack front are not known neither quantitatively nor qualitatively. Hence, the use of local fracture mechanical parameters is not appropriate for the characterization of cracks in elastomeric materials. Therefore, the global energy balance in a specimen undergoing crack propagation seems to be the only candidate for the characterization of fracture in these materials [1]. However, the locations of the processes of energy dissipation are not restricted to the immediate surrounding of the crack front. Moreover, energy dissipation is not only caused by the propagating crack but also by the specific loading conditions. These features complicate the fracture mechanical approach for rubber materials.

Modification of the structure of elastomers influences both the energy dissipation far from the crack front and the fracture process itself. The mechanisms of energy dissipation caused by viscoelasticity [2] and filler reinforcement [3] that occur outside the fracture process zone at small and intermediate strains are understood quite well. In contrast, the processes in the immediate vicinity of the crack front have not been investigated well so far. In that region the material is extensively stretched and the inhomogeneous structure of the material has a pronounced influence on the way the material separation proceeds within the fracture process zone. As it is visible to the naked eye, both the structural changes and the crack velocity influence the resulting fracture surface morphology of elastomeric materials.

In general, surfaces created by fracture are typically irregular and rough. The morphology of fracture surfaces is a signature of the complex fracture process on the scale of microstructure of the corresponding material. Even though roughness varies with different microstructures, its scaling properties are comparable for many materials. Fracture surfaces are found to be self-affine objects that can be described by a universal roughness exponent $\zeta \approx 0.8$ [4]. In contrast, recent studies reveal that these fracture surfaces are anisotropic objects that show different roughness exponents across and along the crack propagation direction. For a wide range of materials including glass, mortar, wood, quasicrystals, and metallic alloys, roughness exponents determined across and along the crack propagation direction are found to be $\zeta \approx 0.8$ and $\beta \approx 0.6$, respectively [5–7]. However, it was found that the fracture surface roughness exponents in glassy ceramics and sandstone are significantly lower: $\zeta \approx 0.4$ and $\beta \approx 0.5$, respectively [8,9], which put the universality of the higher roughness exponents in question. Furthermore, it is found that higher roughness exponents describe the scaling behavior on the length scales of the fracture process zone, where a ductile mechanism prevails. On length scales that are larger than the size of the fracture process zone, the morphology proves to be well described by the smaller roughness exponents [10,11].

II. MATERIALS AND EXPERIMENTAL SETUP

Fracture surfaces of elastomeric materials without fillers or those with low filler content are quite rough at the mac-

---

*horst@ipfdd.de

roscopic length scale, especially when they are formed as a result of slow crack propagation with a low crack velocity. In order to analyze the roughness by means of different methods at different length scales, we use a material that has fracture surfaces that are smooth at the macroscopic length scales.

The results described in this paper are obtained from an emulsion styrene-butadiene rubber (SBR) vulcanizate, which was reinforced with 50 parts (wt %) per hundred rubber (phr) carbon black N330. The matrix was the noncrystallizable statistical styrene-butadiene copolymer SBR 1500 with a styrene content of 23.5%. Cross-linking was performed with a sulfur-accelerator system. The contents of the sulfur and the vulcanization accelerator *N*-cyclohexyl-2-benzothiazole-sulfenamide (CBS) were 1.6 phr. Additionally, 3 phr of the activator zinc oxide were added. The usual content of stearic acid used as vulcanization activator and as processing additive was 1 phr. In addition, 1 phr of an aging protective additive was used. The compound was obtained by using a laboratory mixer. Finally, plates were vulcanized with a vulcanization press at a temperature of 160 °C.

Fracture surfaces were obtained from single edge notched tension specimens. Specimen dimensions were as follows: length $L = 100$ mm, width $W = 25$ mm, and thickness $B = 6$ mm. A notch of 1/4 of the specimen width was produced by a razor blade. The fracture mechanical test was conducted in tension mode under quasistatic loading at 10 mm/min and room temperature. Clamping distance was 40 mm. After short slow stable crack propagation with a crack velocity of order 10^{-6} m/s, the sample was torn in an unstable manner where the crack velocity increases up to five orders of magnitude.

The surfaces resulting from fast crack propagation were analyzed at various length scales by means of atomic force microscopy resolving fine-scale details ranging from nanoscopic to microscopic length scales and optical chromatic distance measurement with a lateral resolution ranging from microscopic to macroscopic length scales. With regard to the characteristic roughness scaling found for fracture surfaces of various materials at length scales smaller than the size of the fracture process zone, the results reported here were obtained on the smallest length scales, i.e., by means of atomic force microscopy, for the analyzed fracture surfaces.

The surfaces were scanned in several 20×20 μm^2 areas with 1024×1024 data points by means of an AFM Q-Scope 250 (Quesant Instrument Corporation, USA) using intermitting mode at 2 Hz scan frequency. The measurement was done far from the notch where the surfaces were created by fast unstable crack propagation and roughness statistics were stationary. Scanning was carried out in both directions, i.e., across and along the crack propagation direction.

III. RESULTS

The frame of reference is chosen so that the unit vectors $\vec{e}_x$ and $\vec{e}_z$ are parallel to the direction of crack propagation and to the crack front, respectively. A typical AFM image of the fracture surface is shown in Fig. 1.

In order to analyze statistical properties of the fracture surface, profiles along and across the crack propagation di-
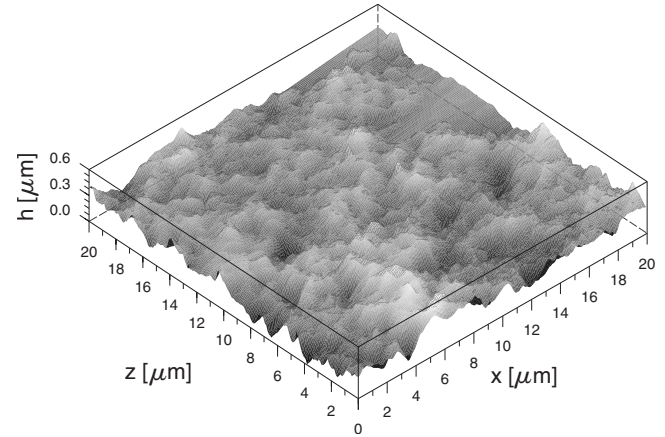

FIG. 1. Atomic force microscopic image of the analyzed fracture surface.

rection were extracted from the surface data. For every profile we calculated the one-dimensional (1D) height-height correlation functions of the order k [12–14],

$$C_k(\Delta r) = \langle |h(r + \Delta r) - h(r)|^k \rangle_r^{1/k}, \tag{1}$$

based on the kth moment of the height fluctuations

$$\Delta h(\Delta r) = |h(r + \Delta r) - h(r)| \tag{2}$$

on a scale Δr. The angular brackets in Eq. (1) denote the average over the profile coordinate r.

In the case of height fluctuations Δh obeying a Gaussian distribution with a self-affine scaling of the variance with Δr, the height-height correlation functions become

$$C_k^G(\Delta r) = (2\Delta r^{2\zeta})^{1/2}\{\Gamma[(k+1)/2]/\sqrt{\pi}\}^{1/k}, \tag{3}$$

with ζ being the roughness exponent. Consequently, the height-height correlation functions (3) normalized by the ratio

$$R_k(\Delta r) = \frac{C_k(\Delta r)}{C_2(\Delta r)} \tag{4}$$

that yields

$$R_k^G(\Delta r) = \sqrt{2} \left\{ \frac{\Gamma[(k+1)/2]}{\sqrt{\pi}} \right\}^{1/k}, \tag{5}$$

in this case, collapse for all k [12]. Deviations from the Gaussian distribution of height fluctuations result in multi-affine scaling regime, i.e., a k-dependent roughness exponent. It was shown that these deviations are due to vertical jump discontinuities in the roughness profile [12–14].

Accordingly, profiles along and across the crack propagation direction of the scanned surface were analyzed by means of

$$C_k(\Delta x) = \langle |h(x + \Delta x) - h(x)|^k \rangle_r^{1/k} \tag{6}$$
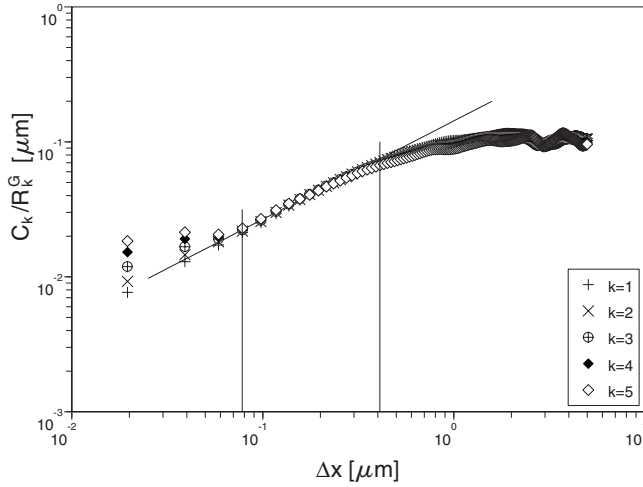
and

FIG. 2. Typical normalized 1D height-height correlation functions for a profile extracted along the crack propagation direction.

$$C_k(\Delta z) = \langle |h(z + \Delta z) - h(z)|^k \rangle_r^{1/k} \qquad (7)$$

both normalized by Gaussian ratio (5). Typical results of the height-height correlation functions normalized by the Gaussian ratio for profiles along and across the crack propagation direction are plotted in Figs. 2 and 3.

It can be seen that roughness exponents, that are independent of k, can be determined within a certain range of length scales. A power-law fit for every profile in the regime between 80 and 400 nm leads to the roughness exponents shown in Table I, where 1024 profiles per AFM image were analyzed along and across the crack propagation direction. Differences in the roughness exponents between both directions are clearly visible in Fig. 4, where $C_2(\Delta x)$ and $C_2(\Delta z)$ are plotted for a typical profile along and across the crack propagation direction, respectively.

It is shown that the analyzed rubber material has anisotropic fracture surfaces described by the average roughness exponents $\zeta = 0.87 \pm 0.03$ along the crack front and
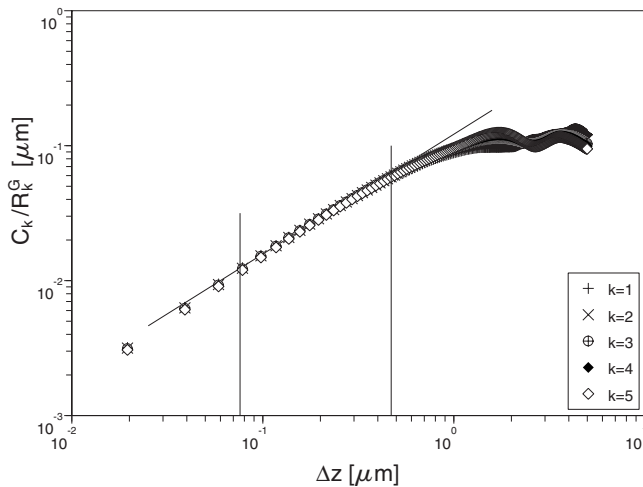
TABLE I. Roughness exponents measured from the calculation of the 1D height-height correlation functions $C_2(\Delta x)$ and $C_2(\Delta z)$ for profiles extracted along and across the crack propagation direction.

AFM image	ζ	β
1	0.84 ± 0.04	0.65 ± 0.06
2	0.86 ± 0.04	0.71 ± 0.08
3	0.84 ± 0.03	0.71 ± 0.05
4	0.89 ± 0.02	0.67 ± 0.05
5	0.85 ± 0.03	0.66 ± 0.05
6	0.88 ± 0.03	0.76 ± 0.05
7	0.91 ± 0.03	0.73 ± 0.06
Average	0.87 ± 0.03	0.70 ± 0.06

$\beta = 0.70 \pm 0.06$ along the crack propagation direction. These values are close to those observed for fracture surfaces of nonrubber materials where the roughness exponents were conjectured to characterize the scaling behavior at length scales within the fracture process zone. As can be seen in Figs. 2 and 3, the upper cutoff length of the indicated scaling regime is about 400 nm for profiles extracted in along the crack front and its propagation direction. The lower cutoff is about 80 nm along the crack propagation direction, as determined by the observed deviation of the height fluctuation distribution from the Gaussian law that results in a multiaffine scaling regime due to vertical jumps in the roughness profiles. In the case of the profiles along the crack front, height fluctuations obey a Gaussian distribution, at least on the scales exceeding that of the lateral resolution of the measurements, which leads to a self-affine scaling. Jump discontinuities can also take place, but their influence is limited to the length scales that are smaller than the lateral resolution of the measurements.

For a complete description of the two-dimensional (2D) features of the fracture surface, the 2D height-height correlation function

FIG. 3. Typical normalized 1D height-height correlation functions for a profile extracted across the crack propagation direction.
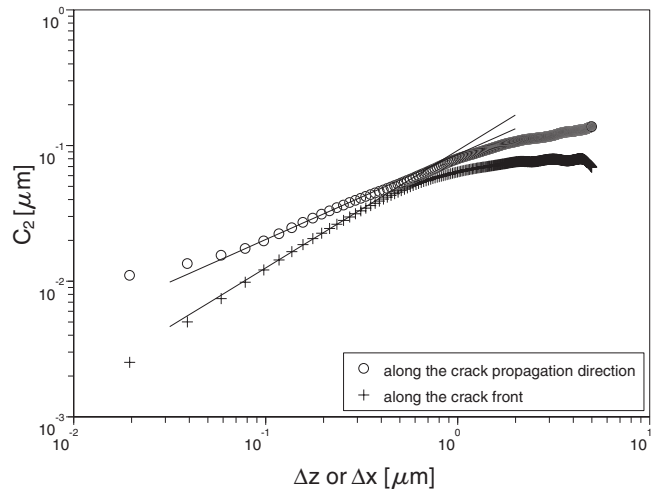

FIG. 4. Typical 1D height-height correlation functions $C_2(\Delta x)$ and $C_2(\Delta z)$ for a profile extracted along and across the crack propagation direction, respectively.
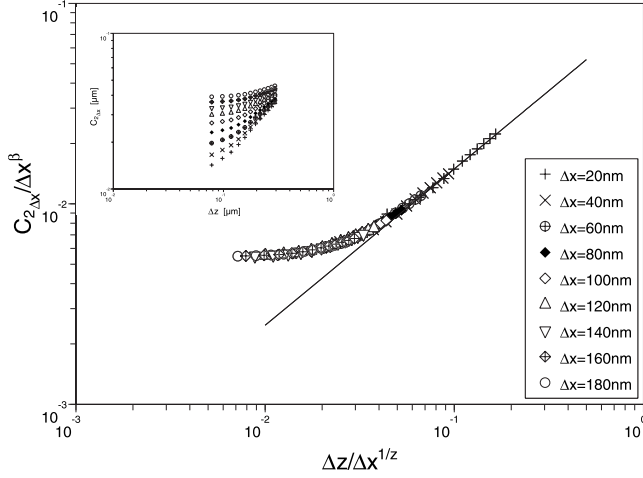
FIG. 5. Typical normalized 2D height-height correlation function. The inset shows the corresponding 1D height-height correlation functions for variations Δz at constant values Δx.

$$C_2^{2D}(\Delta z, \Delta x) = \langle [h(z+\Delta z, x+\Delta x) - h(z,x)]^2 \rangle_{z,x}^{1/2} \qquad (8)$$

was computed for the self-affine regime within the indicated range of length scales. Variations in the 2D height-height correlation function (8) for different fixed values of Δx are shown in the inset of Fig. 5. By normalizing the abscissa and the ordinates by $\Delta x^{1/z}$ and Δx^β, a single master curve can be obtained for specific values of z and β that optimize the collapse of 2D height-height correlation functions for different fixed Δx; see Fig. 5. Hence, similar to fracture surfaces of nonrubber materials [5,10], the elastomeric fracture surface follows a Family-Vicsek scaling [15] within the self-affine regime following

$$C_2^{2D}(\Delta z, \Delta x) \sim \Delta x^\beta f(\Delta z/\Delta x^{1/z}), \qquad (9)$$

where

$$f(u) = \begin{cases} 1 & \text{if } u \ll 1, \\ u^\zeta & \text{if } u \gg 1. \end{cases}$$

The exponents ζ, β, and z refer to the roughness exponent, the growth exponent, and the dynamic exponent. They were determined for all measured height maps, see Table II, where the ratio ζ/β is indicated as well.

TABLE II. Scaling exponents measured from the calculation of the 2D height-height correlation function.

AFM image	ζ	β	z	ζ/β
1	0.84	0.72	1.22	1.17
2	0.89	0.79	1.19	1.13
3	0.78	0.68	1.21	1.15
4	0.93	0.78	1.26	1.19
5	0.89	0.78	1.20	1.14
6	0.98	0.81	1.17	1.20
7	0.93	0.81	1.25	1.15
Average	0.89 ± 0.06	0.76 ± 0.05	1.21 ± 0.03	1.17

Within the self-affine regime, the three exponents are found to be $\zeta = 0.89 \pm 0.06$, $\beta = 0.76 \pm 0.06$, and $z = 1.21 \pm 0.03$. As $z = \xi/\beta$, the 2D scaling properties can be characterized by two scaling exponents within this regime.

IV. DISCUSSION AND CONCLUSION

Since heterogeneities can be found over a wide range of length scales in filled elastomers, it is therefore of high practical interest to estimate the relevant length scales of the fracture process. Here, we determined the scaling exponents for the fracture surfaces formed in the considered highly filled rubber material as a result of fast crack propagation by means of 1D and 2D height-height correlation functions. The exponents were found to be close to those determined for other mostly brittle materials on the length scale where a ductile mechanism prevails. Such a process is related to a microscopic damage mechanism over a limited range of length scales characterized by the formation, growth, and coalescence of voids or microcracks [10,11,16]. Hence, the upper cutoff length of about 400 nm can be used as a rough estimate of the dimension of the fracture process zone within the fracture plane.

The considered material is a weakly cross-linked polymeric system having a high content of carbon black N330. In this material, there is a pronounced polymer-filler interaction that stems from a strong chemical and physical binding due to the roughness of the filler surface [3]. The mean size of primary particles is about 30 nm, but the natural form of the filler consists of primary aggregates with a mean diameter of about 130 nm. Due to high filler content a weakly bonded superstructure is formed from the interpenetrating filler clusters, see Fig. 6, as a result of the flocculation of primary aggregates. Mechanical connectivity between the filler particles that belong to different primary aggregates is provided by a flexible nanoscopic bridge of glassy polymers formed due to the immobilization of the rubber chains close to the gap between different primary aggregates [3].

Moreover, with increasing strain, the stress-induced breakdown of rigid filler clusters occurs due to destroying nanoscopic bridges connecting them. The large strains in the ligament developed during quasistatic loading of the sample before final fast crack propagation induce a total breakdown of the filler network implying cluster sizes of the order of the aggregate size, i.e., 130 nm. Consequently, the concentration
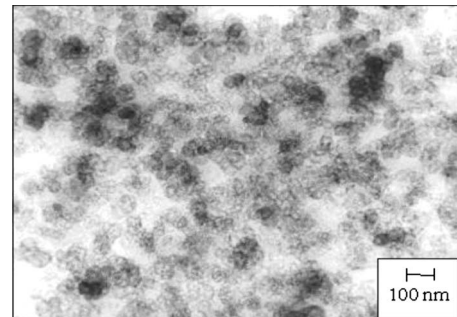

FIG. 6. Transmission electron microscopic image of the SBR vulcanisate with 50 phr N 330 (virgin state).

of destroyed nanoscopic bridges between filler aggregates is quite high due to the high filler content. Therefore, the multiaffine scaling regime on the scales smaller than 80 nm for profiles along the crack propagation direction can be attributed to profile overhangs due to voids developed from destroyed nanoscopic bridges between different filler aggregates.

Even though the investigated part of the fracture surface was created by the fast crack propagation, it should be noted that the fracture occurs in the quasistatic regime; i.e., the stress wave propagation is irrelevant for the fast crack propagation considered here. However, viscoelasticity is essential for capturing the fracture behavior of elastomeric materials [2,17]. Crack velocity influences the local loading rate of the material in the vicinity of the crack front, which has an impact on the deformation mechanism in such polymeric materials. Higher crack velocities induce higher local loading rates in the vicinity of the crack front leading to a glassy deformation of the polymeric chains. In contrast, lower crack velocities trigger lower loading rates in the vicinity of the crack tip leading to a rubbery deformation and, consequently, to extensive deformations even under quite low external forces. In this case, polymeric network chains can align, and finally they are highly stretched and a pronounced elastic crack front blunting can be observed.

The fracture of elastomeric materials is always caused by the loss of integrity of the material in the fracture process zone; thus, the rupture of overloaded polymeric network chains is its basic requirement. Hence, the deformation mechanism of polymeric chains in the vicinity of the crack front influences the fracture process. For the case considered, polymeric chains in the ligament far from the crack tip are moderately stretched during quasistatic loading of the sample. However, further local loading due to the fast propagation of the crack implies a high local loading rate in the vicinity of the crack front and, thus, a glassy deformation

behavior and a corresponding overloading of chains in nonequilibrium. Nonetheless, with increasing the distance from the crack tip, local loading rates decrease, which results in viscoelastic energy losses. Consequently, even though the amount of the tearing energy as fracture mechanical parameter [1] is governed by viscoelastic losses outside the fracture process zone [18], the fracture process itself seems to be driven by the glassy behavior of moderate prestrained polymeric chains at short times.

In contrast, owing to the presence of large entropic deformations of the polymer network chains at slow crack propagation, blunting effects become important, which cause a different crack mechanism that results in the formation of a discontinuous crack front observed also for other soft materials such as gelatine [19]. Due to discontinuous crack front, characteristic cross-hatched patterns can often be observed in this case. The appearance of a transition from a cross-hatching fracture surface morphology at slow fracture to a smoother fracture surface at fast fracture is therefore related to the molecular dynamics of polymeric chains resulting in a different fracture process for both cases. In order to study the peculiarities of these fracture mechanisms, the change in molecular dynamics due to a decreased mobility of highly stretched polymeric chains and consequently the change in relaxation properties at large deformations must be taken into account [20].

[1] R. S. Rivlin and A. G. Thomas, J. Polym. Sci. **10**, 291 (1953).

[2] B. N. J. Persson, O. Albohr, G. Heinrich, and H. Ueba, J. Phys.: Condens. Matter **17**, R1071 (2005).

[3] M. Klüppel, Adv. Polym. Sci. **164**, 1 (2003).

[4] E. Bouchaud, G. Lapasset, and J. Planés, Europhys. Lett. **13**, 73 (1990).

[5] L. Ponson, D. Bonamy, and E. Bouchaud, Phys. Rev. Lett. **96**, 035506 (2006).

[6] L. Ponson, D. Bonamy, H. Auradou, G. Mourot, S. Morel, E. Bouchaud, C. Guillot, and J. P. Hulin, Int. J. Fract. **140**, 27 (2006).

[7] L. Ponson, D. Bonamy, and L. Barbier, Phys. Rev. B **74**, 184205 (2006).

[8] L. Ponson, H. Auradou, P. Vié, and J. P. Hulin, Phys. Rev. Lett. **97**, 125501 (2006).

[9] L. Ponson, H. Auradou, M. Pessel, V. Lazarus, and J. P. Hulin, Phys. Rev. E **76**, 036108 (2007).

[10] D. Bonamy, L. Ponson, S. Prades, E. Bouchaud, and C. Guillot, Phys. Rev. Lett. **97**, 135504 (2006).

[11] L. Ponson, Ann. Phys. **32**, 1 (2007).

[12] S. Santucci, K. J. Måløy, A. Delaplace, J. Mathiesen, A. Hansen, Jan Ø. H. Bakke, J. Schmittbuhl, L. Vanel, and P. Ray, Phys. Rev. E **75**, 016104 (2007).

[13] M. J. Alava, P. K. V. V. Nukala, and S. Zapperi, J. Stat. Mech.: Theory Exp. (2006) L10002.

[14] S. J. Mitchell, Phys. Rev. E **72**, 065103(R) (2005).

[15] F. Family and T. Vicsek, *Dynamics of Fractal Surfaces* (World Scientific, Singapore, 1991).

[16] D. Dalmas, A. Lelarge, and D. Vandembroucq, Phys. Rev. Lett. **101**, 255501 (2008).

[17] T. Horst and G. Heinrich, Polym. Sci., Ser. A **50**, 583 (2008).

[18] K. Tsunoda, J. J. C. Busfield, C. K. L. Davies, and A. G. Thomas, J. Mater. Sci. **35**, 5187 (2000).

[19] T. Baumberger, C. Caroli, D. Martina, and O. Ronsin, Phys. Rev. Lett. **100**, 178303 (2008).

[20] M. Febbo, A. Milchev, V. Rostiashvili, D. Dimitrov, and T. A. Vilgis, J. Chem. Phys. **129**, 154908 (2008).